Iron-Loaded Carbonized Spent Bleaching Earth (Fe-SBE/C) Composite Used for Arsenic Removal from Water

Siswanti Puji , Juntao Guo , Yihui Zhang , Kexin Song , Feng Wu * , Jing Li *

Posted Date: 12 February 2024

doi: 10.20944/preprints202402.0685.v1

Keywords: arsenic; adsorption; spent bleaching earth; low-cost adsorbent

Article

Iron-Loaded Carbonized Spent Bleaching Earth (Fe-SBE/C) Composite Used for Arsenic Removal from Water

Siswanti Puji [1], Juntao Guo [1], Yihui Zhang [1], Kexin Song [1], Feng Wu [1,*] and Jing Li [2,*]

[1] Hubei Key Lab of Biomass Resource Chemistry and Environmental Biotechnology, School of Resourcess and Environmental Science, Wuhan University, Wuhan, 430079, China
[2] Central-South Architectural Design Institute Co., Ltd. (CSADI), Wuhan, 430071, China
* Correspondence: fengwu@whu.edu.cn (F.W.); 327266781@qq.com (J. L.)

Abstract: For the last two decades, an increasing demand for low-cost adsorbents for drinking water treatment has been challenged in the rural areas of developing countries that have problems with arsenic (As) contamination. In this work, spent bleaching earth (SBE), a residual material that is formed during the process of refining vegetable oil, has been utilized to prepare the new magnetic adsorbent Fe-SBE/C by modifying its surface area through calcination and co-precipitation with iron. The experimental results demonstrate that Fe-SBE/C exhibits a substantial adsorption capacity towards both arsenite (As(III)) and arsenate (As(V)). Optimal pH conditions were found to be pH 10 for As(III) and pH 3 for As(V), resulting in adsorption percentages of 76.7% and 94.1%, respectively. Other experimental parameters such as calcination conditions, adsorbent dosage, iron-loading ratio, and the presence of co-existing ions were thoroughly investigated. The kinetic study revealed that the adsorption processes follow the Elovich and intraparticle diffusion models, suggesting a combined adsorption mechanism of boundary layer control and chemisorption. Furthermore, the isotherm followed the Langmuir model with a maximum adsorption capacity of 202.61 μg g-1 for As(III) and 187.61 μg g-1 for As(V). Through thermodynamic analysis and reinforcement by activation energy data, this research validates that the observed adsorption process is indicative through chemisorption. The regeneration study revealed the potential for multiple cycles of arsenic removal, highlighting the practical applicability of Fe-SBE/C in environmental contexts. In conclusion, the findings of this study underscore the efficacy of Fe-SBE/C in arsenic removal and present it as a promising and environmentally friendly solution for mitigating arsenic pollution.

Keywords: arsenic; adsorption; spent bleaching earth; low-cost adsorbent

1. Introduction

Arsenic (As) is one of the most poisonous elements that exist naturally. This metal's toxicity threatens the environment as it accumulates in organisms inhabiting streams, resulting in detrimental health effects for humans, plants, and animals [1–3]. Prolonged ingestion of arsenic through drinking water is correlated with the development of arsenicosis, a condition characterized by various types of cancer, high blood pressure, neurological complications, and cardiovascular disease [4]. Approximately 220 million people worldwide are classified as direct consumers of water contaminated with As [5]. The primary population at risk from arsenic consumption consists mainly of individuals from Asian countries. Elevated arsenic levels have been observed in several nations, notably India, Bangladesh, Nepal, China, and Indonesia. The World Health Organization (WHO) has established the guideline of the permissible arsenic concentration level in drinking water at 10 μg/L, which has been endorsed by most nations worldwide [6].

Arsenic exists in the environment as an organic and inorganic species, with the latter being significantly more toxic [7]. In aqueous environments, inorganic arsenic is typically found in trivalent state (As(III)) and pentavalent state (As(V)). Owing to its chemical stability, As(V) tends to be more prevalent than As(III) in natural waters with pH levels ranging from 4 to 8. In contrast, in anaerobic groundwater with a pH less than 9, As(III) is often more commonly found [8]. As(III) is considered

 doi:10.20944/preprints202402.0685.v1

more hazardous than As(V) from a health and ecological perspective. Recently, there has been a significant surge in research to remove arsenic from various environments effectively. Various techniques, including oxidation [9], coagulation or electrocoagulation [10], ion exchange [11], adsorption [12], photocatalysis [13], and membrane technologies [14], are employed to remove pollutants from groundwater or surface water efficiently. Adsorption has emerged as the prevailing choice for arsenic mitigation due to its less production of undesirable byproducts and high potential compared to other existing methods. Furthermore, the adsorbent can be regenerated multiple times for subsequent use. Moreover, it is widely acknowledged in practical scenarios for its user-friendly operation, energy efficiency, and exceptional removal effectiveness [15,16]. An appropriate adsorbent for eliminating arsenic from water should possess good affordability, effectiveness, and ecological compatibility. Cheap local materials (e.g., clay, charcoal, Fe-containing minerals, etc.) are desirable in the rural areas of developing countries. Moreover, combining composites based on clays confers a significant benefit compared to using natural clay alone. For instance, Mukhopadhyay et al. [17] employed Fe-modified smectite to eliminate As from aqueous solutions. Baigorria et al. [12] employed Fe(III)-modified bentonite for arsenic adsorption in an aqueous system. Spent bleaching earth (SBE) has recently been widely used to eliminate heavy metals or organic pollutants from water-based systems. As a residual substance from the process of refining vegetable oil, SBE consists of approximately 65-75% SiO2, 20-40% residual oil, and 15-20% Al_2O_3 [18]. Removing and disposing of SBE is challenging due to its elevated oil content. SBE was deposited in landfills for many years without undergoing specific treatment. Nevertheless, its viability has been compromised due to its potential environmental hazards, such as fire risk and unpleasant odors [19]. Researchers have developed methods to repurpose it as a potential adsorbent over the last few decades instead of using it directly. Eko Saputro et al. [20] successfully regenerated the SBE by subjecting it to oil extraction and high-temperature calcination, enabling its reuse in oil refining. Tang et al. [21] have produced attapulgite/carbon through a single-step calcination process using SBE, resulting in a highly effective adsorbent for Pb(II). Liu. et al. [22] produced a clay-activated carbon material capable of absorbing Pb(II) by subjecting SBE to carbonization and subsequently activating it with potassium hydroxide. Wan et al. synthesized a clay/carbon composite (SBE/C) through one-step pyrolysis under a N2 atmosphere to effectively eliminate tetracycline hydrochloride in aqueous solutions[23] and bisphenol A [24] from wastewater. It is well known that iron oxide can be effectively immobilized on porous material for adsorbent, including bentonite, kaolinite, carbon, and zeolite. Liu et al. [25] and Chen et al. [26] have modified SBE into a magnetic Fe-SBE composite that can effectively remove organic pollutants from wastewater, such as tetracycline hydrochloride and bisphenol A. For As adsorption, incorporating iron, mainly Fe(III), into the structure of the adsorbent material is critically important [27–31]. Fe(III) contributes to the formation of effective arsenic adsorption sites. The interaction between iron and arsenic can manifest through various mechanisms, including the formation of monodentate and bidentate complexes, ligand exchange processes, or electrostatic attraction [32]. Accordingly, the iron modification on SBE-based adsorbents for removing arsenic could have yielded exceptional outcomes. However, no attempt to use Fe-SBE to eliminate arsenic has been reported. This study utilized SBE as the initial material to produce SBE/carbon (SBE/C) through calcination. Subsequently, the modification of SBE/C with iron to the composite Fe-SBE/C was conducted through the co-precipitation technique. The Fe-SBE/C material was explicitly developed for As(III)/As(V) adsorption, marking its inaugural use. The adsorptive properties of Fe-SBE/C were explored in detail, focusing on the impact of critical factors such as pH, adsorbent dose, arsenic concentration, temperature, duration of calcination, and the presence of other ions on As(III)/As(V) adsorption. In addition, the adsorption process has been thoroughly investigated with various characterization, thermodynamic, and kinetic analyses. This work provides a cheap and practical adsorbent for arsenic removal from water and a new utilization strategy of SBE for developing countries.

 doi:10.20944/preprints202402.0685.v1

2. Results and Discussion

2.1. Physicochemical Characteristics of the Adsorbent

2.1.1. Fourier Transform Infrared Spectra

Figure S1 displays the Fourier transform infrared spectra (FTIR) spectra of the raw and modified material, including VBE, SBE, SBE/C and Fe-SBE/C at different calcination temperatures (350 - 550 °C). The adsorption bands of the virgin bleaching earth(VBE), SBE/C, and Fe-SBE/C show a similar pattern to SBE except at bands 2917 and 2849 cm^{-1}. These two bands indicate the presence of -CH_3, -CH_2-, and C-H group bands [33]. This contrast highlights the presence of palm oil after the virgin-bleaching earth has absorbed it. After calcination, these absorption bands no longer exist, thus proving that the residual substance, specifically palm oil, transforms into carbon species during the calcination process. A solitary peak is observed at a wavenumber of 543 cm^{-1}, indicating the stretching mode of Fe-O in Fe_3O_4. Magnetite particles (Fe_3O_4) can be attributed to the absorption bands observed within the 475 to 1600 cm^{-1} spectral range, specifically at 440, 795, 1027, 1456, and 1634 cm^{-1} [16]. Furthermore, the FTIR analysis confirms the chemical stability of all functional groups in the material and verifies that the iron was successfully loaded into the SBE/C.

2.1.2. The X-ray Diffraction Pattern

VBE, SBE, SBE/C, and Fe-SBE/C, with different SBE: Fe ratios (w/w) and at different calcination temperatures, were examined for the X-ray diffraction (XRD) pattern (Figure 1). Based on the observed pattern, quartz might be inferred as the main component in this bleaching earth. The diffraction peaks corresponding to quartz are detected at 2θ angles of 20.9, 26.5, and 49.9. The peaks attributed to montmorillonite were detected at 2θ values of 19.8, 29.7, and 34.8. The peaks detected at 2θ = 25.2 and 28.3 can be ascribed to quartz, whereas those observed at 2θ = 30.2 and 35.4 are linked to magnetite [34].

Upon comparing the peak shapes of quartz and montmorillonite, it is evident that they display distinct sharp characteristics in VBE, SBE, and SBE/C. Nevertheless, in Fe-SBE/C, the peak corresponding to the spent bleaching earth component has diminished, resulting in only magnetite peaks characterized by a distinct and well-defined shape. The XRD pattern confirms that the magnetite particles were successfully deposited onto the spent bleaching earth/carbon surface, which indicates a favorable distribution.

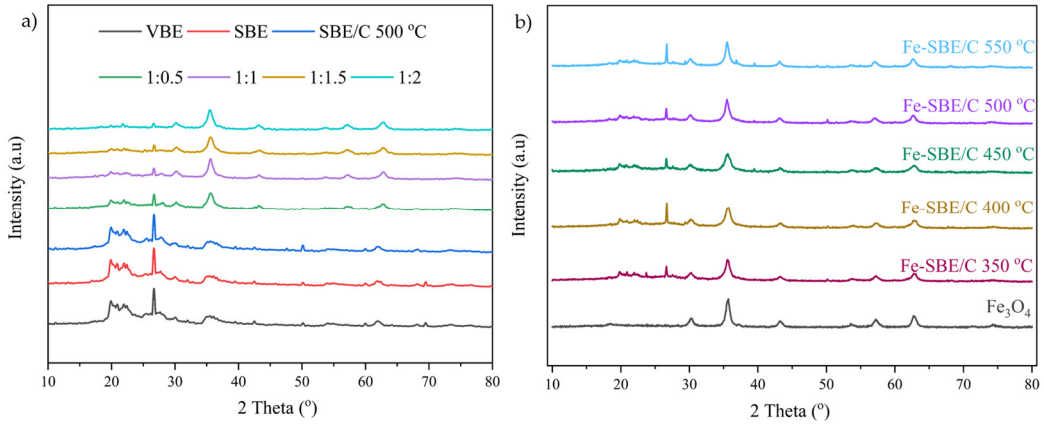

Figure 1. X-ray diffraction of materials for the variation of (**a**) iron ratio and (**b**) calcination temperature.

2.1.3. Field Emission Scanning Electron Microscope and Energy Dispersive Spectroscopy

The Field emission scanning electron microscope (SEM) images (at magnifications of ×10,000 and ×2,000, respectively) of the SBE, SBE/C, and Fe-SBE/C 500 °C-2h sample before the adsorption of arsenic are presented in Figure 2. The materials exhibited porosity, which defined their structure. The

 doi:10.20944/preprints202402.0685.v1

SEM image unequivocally illustrates the existence of surface irregularities in the SBE. Furthermore, the SBE/C exhibits a smooth surface with a distinct sheet-like structure, while the Fe-SBE/C experiences roughening following the iron modification. The roughening process is distinguished by clustered nano-spherical particles resulting from merging iron nanoparticles. Furthermore, there is a noticeable rise in the number of pores, resulting in the surface area having a proportional augmentation. The heightened surface roughness of Fe-SBE/C could potentially lead to a larger adsorption area for As.

Figure S2 and Table 1 present the results of the energy dispersive spectroscopy (EDS) examination, which shows that the materials contain a substantial quantity of the main elements, C, O, Fe, Si, and Al. The proportion of these five elements in each material in SBE/C and Fe-SBE/C, while compared to SBE, changed to a distinct extent. The most significant change was observed in the component C, which decreased from 22.21% to 8.57% and 9.84%, respectively. The observed decrease in the element C can be attributed to the generation of gas and cracking of organic compounds during the pyrolysis process at 500 °C [35].

The primary element, except O, of the Fe-SBE/C is Fe, which constitutes 20.98% of the composite. The contrasts of observed Fe content in the SBE (0.36%) and SBE/C (1.68%) prove that the SBE/C structure has been loaded with Fe [24]. Nevertheless, there is no discernible proof of the existence of As(III) on the surface area after adsorption. As a result of its diminished concentration of only 30-40 μg L^{-1}, the existence of As was not easily detected as anticipated. An alternative explanation for undetected As could be incorporated within the adsorbent's matrix, particularly in its pores. This hypothesis is corroborated by SEM imagery, which depicts the adsorbent's surface as rough and porous, with characteristics conducive to the entrapment of As species within the material's structure.

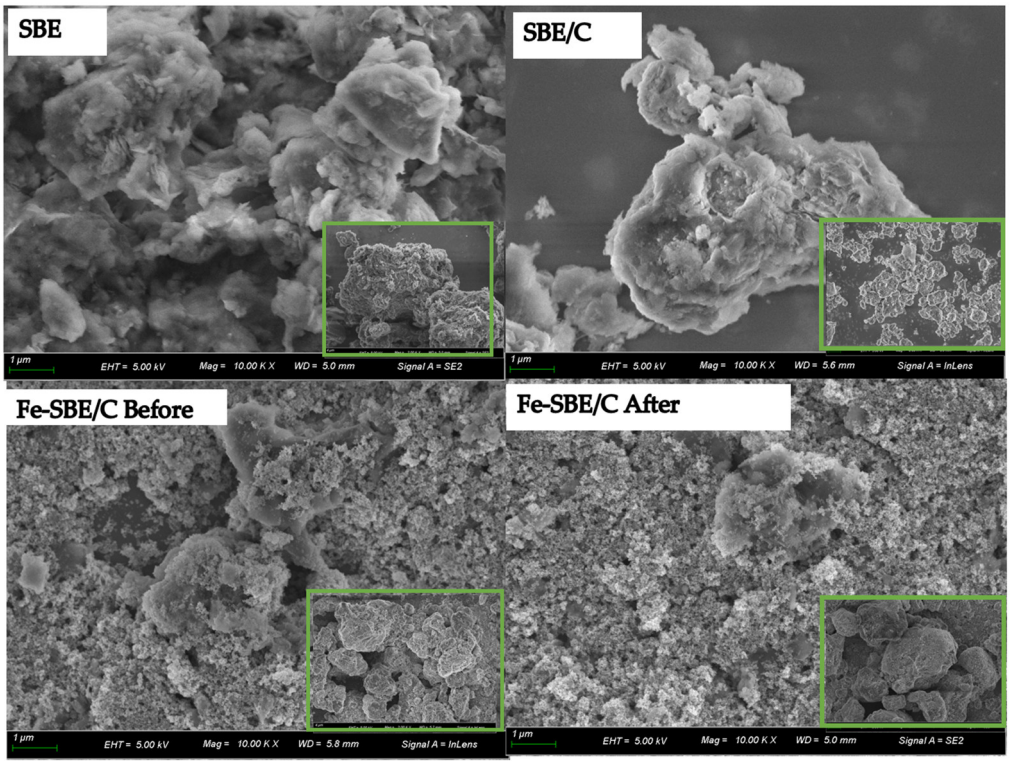

Figure 2. The SEM images of (**a**) SBE, (**b**) SBE, (**c**) Fe-SBE/C before reaction, and (**d**) Fe-SBE/C after reaction.

 doi:10.20944/preprints202402.0685.v1

Table 1. EDS data of SBE, SBE/C, Fe-SBE/C and Fe-SBE/C before and after adsorption.

Materials	Element content (%)				
	C	O	Fe	Si	Al
SBE	22.21	65.88	0.36	7.33	3.29
SBE/C 350 °C	11.81	64.76	1.84	15.49	2.2
SBE/C 400 °C	13.86	64.53	3.93	10.89	3.94
SBE/C 450 °C	12.46	65.74	0.69	16.23	3.07
SBE/C 500 °C	8.57	65.17	1.68	17	4.58
SBE/C 550 °C	9.69	65.23	1.46	15.11	5.55
Fe-SBE/C 350 °C	13.34	62.41	12.3	10.1	1.1
Fe-SBE/C 400 °C	10.82	61.65	14.25	11.17	1.41
Fe-SBE/C 450 °C	10.08	62.98	10.42	14.73	1.11
Fe-SBE/C 500 °C	9.84	59.36	20.98	6.82	1.88
Fe-SBE/C 550 °C	9.81	61.58	14.62	11.76	1.21
Fe-SBE/C 500 °C after Adsorption	10.74	60.52	17.44	8.32	1.91

2.1.4. The BET Surface Area and Distribution of Pore Size

Figure S3a,b depict the nitrogen (N_2) adsorption-desorption isotherms and pore size distribution of the studied materials, respectively. Table 2 displays the measured specific surface area at 191.19, 3029.9, and 2865.7 $m^2 g^{-1}$ for the SBE, SBE/C, and Fe-SBE/C material, respectively. Notably, the SBE demonstrates a lower surface area and total pore volume, which indicates its potential effectiveness in adsorbing organic compounds, such as oil and grease, in the context of the palm oil bleaching process within a refinery system. Furthermore, the observed increase in the surface area of SBE/C post-calcination suggests that this thermal process effectively enhances the material's surface area, potentially improving its adsorption capacities of As.

Table 2. The BET analysis data for SBE, SBE/C and Fe-SBE/C.

Materials	Specific surface area ($m^2 g^{-1}$)	Total Pore volume ($cm^3 g^{-1}$)	Average pore size (nm)
SBE	191.19	1.4716	30.789
SBE/C 500 °C	3029.9	6.913	9.1266
Fe-SBE/C 500 °C	2865.7	8.6964	12.138

2.1.5. Thermogravimetric Analysis

The presence of carbonaceous materials is determined for both the raw and modified materials subjected to TG for mass loss analysis. The SBE, SBE/C, and Fe-SBE/C thermogravimetric curves are depicted in Figure 3a. The calcination process of the SBE was conducted at varying temperatures from (350 - 550 °C) in the air atmosphere for this work. The curve indicates a gradual mass loss (a.u 6.86%) for SBE below 200 °C. This can be attributed to the elimination of physically adsorbed water molecules in the outer surface or inside the structural channels of SBE and zeolitic water. Subsequently, SBE exhibits a significant mass loss (a.u 27.34%) in the range of 200 - 700 °C, primarily due to the combustion of organic compounds trapped within the porous structure of SBE. As the temperature increases, there is a noticeable decrease in the mass loss of SBE composites, indicating a gradual reduction in the carbon content of the composites. It is followed by a steady mass loss (a.u 1.76%) between 700 - 1000 °C, suggesting that the decrease in organic compounds in SBE has ceased and the composite has reached a stable state. In contrast, a decline in mass loss (a.u 12.29%) from 0 -

 doi:10.20944/preprints202402.0685.v1

1000 °C was exhibited for the material SBE/C and Fe-SBE/C, indicating their stability after heat treatment and Fe modification and the absence of organic compounds in the composites. The composite synthesized at 500 °C calcination shows better As removal properties which is shown in the section 2.2.

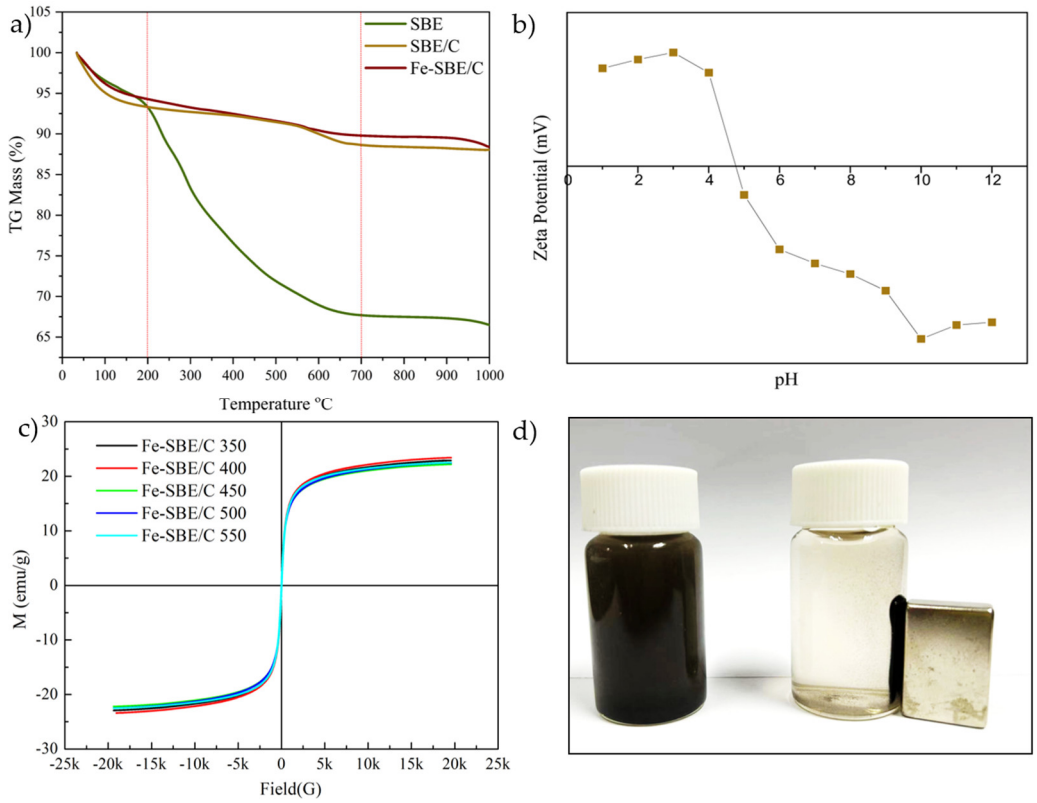

Figure 3. (**a**) TG analysis curve of the SBE, SBE/C 500 °C.2h, and Fe-SBE/C 500 °C.2h. (**b**) pHPZC of Fe-SBE/C. (**c**) The curves of Fe-SBE/C magnetization in different temperature. (**d**) Pictures of Fe-SBE/C in the solution with and without the magnet.

2.1.6. pH_{PZC} Analysis

The pH at which the surface of Fe-SBE/C carries no net charge, known as the pH point of zero charge (pH_{PZC}), was determined and illustrated in Figure 3b. The observed pH_{PZC} was established to be 4.40. The specific pH value signifies a critical juncture at which the net surface charge of Fe-SBE/C transitions. When the solution pH is below 4.40, the Fe-SBE/C's surface exhibits a positive charge, while it becomes negatively charged at a pH value exceeding 4.40. Based on these findings, the variation in the PZC indicates the potential for differential adsorption capacities, affecting the material's affinity for various charged species in a solution, thereby influencing its efficacy in adsorption-based applications.

2.1.7. Magnetic Hysteresis Curves

Figure 3c shows the magnetic hysteresis curves of five materials Fe-SBE/C obtained at different temperatures. The curves display that the saturation of magnetization Fe-SBE/C is 22.45 emu g^{-1}. These curves approach the origin of the coordinate axis, suggesting minimal remanence and coercivity. Consequently, Fe-SBE/C can be classified as a paramagnetic substance, aligning with the findings of Mu and Wang [36]. Additionally, an experiment assessed the solid-liquid separation efficiency of Fe-SBE/C when immersed in purified water for five minutes while subjected to an external magnet. It demonstrates (Figure 3d) that the Fe-SBE/C has strong magnetic properties, which enable rapid separation from the aqueous medium through magnetic intervention. This quality eliminates the need for frequent centrifugation during the material's recycling process, leading to an

 doi:10.20944/preprints202402.0685.v1

extended lifespan, reduced operational expenses, and significant potential for practical applications in environmental and industrial settings.

2.2. Adsorption Study on the Fe-SBE/C

2.2.1. Influence of Calcination Conditions

The Fe-SBE/C composites were employed as adsorbents for treating water containing As(III)/As(V) under controlled experimental conditions. The adsorption abilities of the Fe-SBE/C composites in calcination temperature are illustrated in Figure 4a,b for As(III) and As(V), respectively. As depicted in Figure 4a,b, both As(III) and As(V) adsorption exhibits a notable enhancement in the removal effectiveness with an increase in the calcination temperature of the SBE/C. This observation is supported by the data obtained from EDS analysis, which reveals that the Fe-SBE/C sample treated at 500 °C for 2 hours exhibited a higher Fe loading. The adsorption process in this context involves the utilization of Fe to adsorb arsenic.

Effects of the holding time of calcination (1, 2, and 3 hours) on As(III) and As(V) removal are shown in Figures 4c and 4d, respectively. There is no significant difference in the adsorption efficiency of As(III) in Figure 4c. However, increasing the holding time exhibits significant enhancement of the adsorption efficiency of As(V) in the same experimental initial pH. The results suggest that adsorbents subjected to more extended periods of calcination may exhibit comparable composition. However, the materials, including SBE/C, Fe_3O_4, and Fe-SBE/C, display a significant disparity in their adsorption rate (see Figure S4). This discrepancy can be attributed to the different levels of Fe content present in each material. Specifically, SBE/C contains a mere 1.68% Fe (See Table 1), while Fe-SBE/C possesses a considerably higher Fe content of 20.98%, and there is 72.41% Fe content in Fe_3O_4. Therefore, based on the provided data, it can be deduced that incorporating SBE/C and Fe_3O_4 into the Fe-SBE/C composite material improves its adsorption efficiency of As.

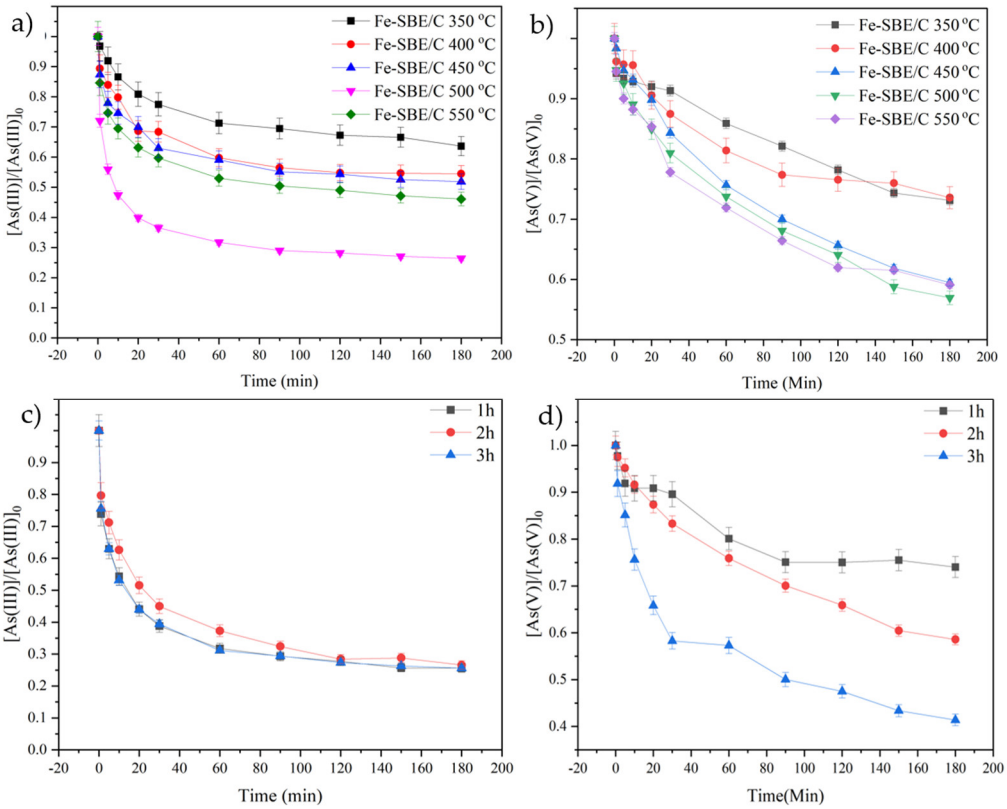

Figure 4. Effects of calcination temperature (**a**,**b**) and calcination holding time (**c**,**d**) on As(III) and As(V) adsorption . Experimental conditions: Adsorbent dosage = 1 g L^{-1}, initial concentration of arsenic = 50 μg L^{-1}, pH = 7, T = 25°C, S= 250 rpm, t= 3 h.

 doi:10.20944/preprints202402.0685.v1

2.2.2. Influence of the Initial pH of Solutions

The experimental investigation of the impact of initial pH on both As(III) and As(V) adsorption was carried out with a batch experiment. The pH levels varied between 3 to 10, and the outcomes indicating the percentage of As elimination concerning the initial pH are presented in Figure 5a,b. Notably, pH has no obvious influence on the adsorption removal of As(III), especially in the pH range 5 – 10; the removal efficiency for As(III) ranged from 60.24-76.73%. On the contrary, As(V) adsorption was heavily influenced by pH; the highest removal efficiency of As(V) was 94.1% at pH 3.0, and the lowest one was only 10.43% at pH 10.

The observed trend in the removal of As can be explained by examining the speciation of As in aqueous solution along with the pH_{PZC}. The pH_{PZC} of Fe-SBE/C, as shown in Figure 3b, is determined to be 4.4. The surface of Fe-SBE/C is positively charged at the pH below 4.4 and negatively charged beyond 4.4. Over a wide range of pH 2 - 8, As(III) remains primarily neutral as $As(OH)_3$, and anion form $O\text{-}As\text{-}(OH)_2^-$ at pH 9 – 12. no dominant repulsive force exists between the Fe-SBE/C and As(III) in terms of charge, allowing for As(III) adsorption onto Fe-SBE/C. While As(V) exists mainly in different anion forms over a wide pH range of 3 – 11, more precisely, $H_2AsO_4^-$ ($O{=}As\text{-}(OH)_2O^-$) at pH 3 - 6, and $HAsO_4^{2-}$ ($O{=}As\text{-}(OH)O_2^{2-}$) at pH 7 – 11. The electrostatic attraction is thought to be less important for As(III) but much more important for As(V) at pH below 4.4 since the lowest As(III) adsorption but highest As(V) adsorption were observed at pH 3, where the surface of Fe-SBE/C is positively charged. Moreover, the electrostatic repulsive force between anions of As and the negatively charged surface of Fe-SBE/C was only observed for As(V) rather than As(III) at pH 10. Therefore, electrostatic adsorption could not be the predominant mechanism for As(III) adsorption on Fe-SBE/C.

According to Morin et al. [37], As(III) removal occurs through surface complexation and ligand exchange processes. They propose that the magnetite surface contains unoccupied tetrahedral sites capable of hosting As(III) by forming stable tridentate, hexanuclear, corner-sharing surface complexes. Additionally, a portion of As(III) can precipitate as an amorphous Fe-As complex on the magnetite surface. In the ligand exchange process, surface hydroxyl groups (OH^-) are replaced by As(III) ions. The abundance of surface hydroxyl groups increases with higher pH, contributing to enhanced removal of As(III) at elevated pH levels [38–40]. Accordingly, $As(OH)_3$ has a strong complexing ability due to having 3 OH^-. Surface complexation may also play an important role in the As(V) adsorption similar to As(III) in nature. From this viewpoint, $H_2AsO_4^-$ may have a stronger complexing ability than $HAsO_4^{2-}$. While in terms of electrostatic interaction, $HAsO_4^{2-}$ has a higher charge density than $H_2AsO_4^-$, thus has a stronger repulsive force with Fe-SBE/C surface at pH 10. Consequently, the less negative charge of As(III) and the favourable electrostatic and interactions involving chemical substances along the positively charged adsorbent surface make the adsorption of As(III) more efficient in near-neutral pH conditions despite the adsorbent's pH_{PZC} of 4.4 [41].

 doi:10.20944/preprints202402.0685.v1

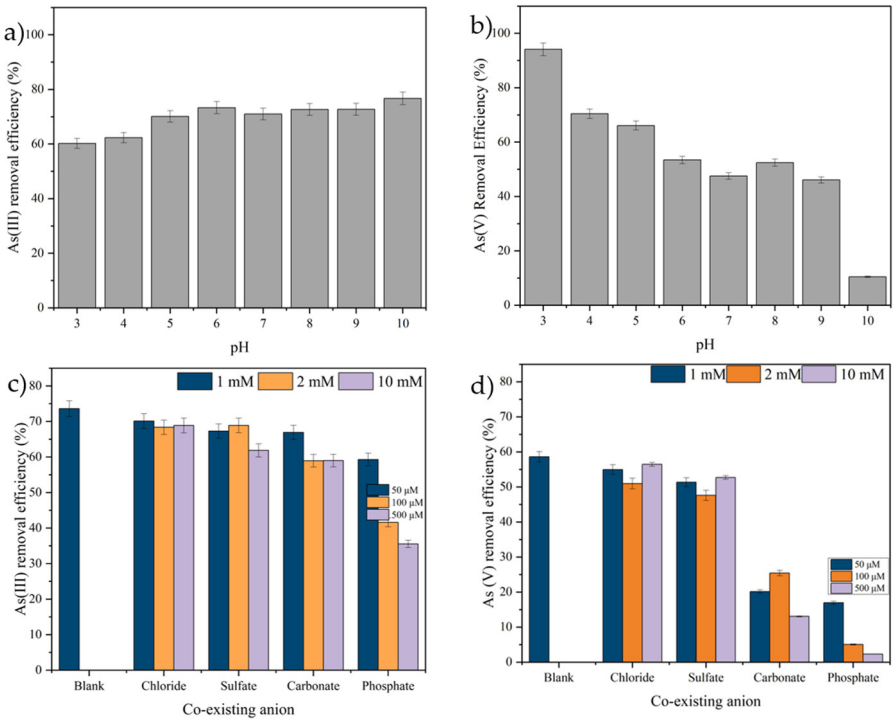

Figure 5. Effects of the initial pH and co-existing ions on the adsorption of As(III) (**a**,**c**) and As(V) (**b**,**d**). Experimental conditions: Adsorbent dosage = 1 g L^{-1}, Initial concentration = 50 μg L^{-1}, pH = 3-10, T = 25°C, S= 250 rpm, t= 3 h.

2.2.3. The Influences of Dosage and Iron Ratio of Fe-SBE/C

The adsorbent dosage and iron ratio influences on arsenic adsorption are illustrated in Figure S5. The quantity of the adsorbent employed significantly impacts the adsorption efficiency of an adsorbent. Theoretically, augmenting the dosage of the adsorbent results in a rise in the abundance of active sites that are accessible for the adsorption of arsenic ions. This study examined the adsorbent concentration in the 0.5 to 2 g L^{-1} range. The removal efficiency of arsenic ions increased with higher dosages of Fe-SBE/C. Consequently, this should improve the adsorption capacity [42]. As shown in Figure S5a,c, the adsorption efficiency of both As(III) and As(V) increased proportionally with higher concentrations of Fe-SBE/C. The increase in the total number of adsorbable sites can be attributed to the application of higher dosages.

The experimental results demonstrate the adsorption of As(III) and As(V) with varying Fe(III): Fe(II) molar ratios (0.5:0.5, 1:1, 1.5:1.5, and 2:2) in the Fe-SBE/C composite. In Figure S5b, the results demonstrate an initial rise in removal efficiency of As(III), followed by a subsequent decline as the Fe(III): Fe(II) molar ratio increases. Specifically, the molar ratio 1.5:1.5 demonstrates superior adsorption performance for As(III) adsorption. On the other hand, the ratio of Fe(III): Fe(II) has little influence on As(V) adsorption at the optimal pH, with Fe(III): Fe(II) of 2:2 displaying a slightly higher adsorption rate.

2.2.4. The Influence of Co-Existing Ions

Other ions can influence the mechanism and efficiency of As removal in the water matrix. The existing literature has demonstrated that multiple anions in the As solution reduce the adsorbent's adsorption capacity [43]. In this work, impacts of common anions including chloride, sulfate, carbonate, and phosphate were examined on As adsorption. Results in Figure 5c,d reveal that adding these ions leads to different extent of decreases in As adsorption. Sulfate ions cause an 11.7% decrease in As(III) concentration at higher concentrations, with phosphate ions having a more significant impact on As(III) adsorption due to competition for adsorption sites. Chloride ions have a minimal effect on As(III) adsorption, resulting in only a 4.7% reduction at higher concentrations, likely due to

 doi:10.20944/preprints202402.0685.v1

their negative charge [44]. In a similar context, a highly significant decrease in the presence of As(V) was observed, especially with a reduction of 38.1% by phosphate ions and 14.6% by bicarbonate ions, whereas the addition of chloride and sulfate ions showed no significant impact. The similar charge and size of phosphate, bicarbonate, and As may result in comparable ionic behavior when interacting with Fe-containing adsorbents [45].

2.2.5. Adsorption Kinetics

This study aimed to investigate the kinetics of As(III) and As(V) removal by utilizing the pseudo-first-order, Elovich, and intra-particle diffusion models, respectively. The pseudo-second-order model was not considered in this work since there has been debate on its rationality [46,47]. The obtained results from these models are depicted in Figure S6. The regression coefficient (R^2) and the calculated parameters from these models are compared to the experimental values. As shown in Table 3, adsorptions of As(III) and As(V) follows the pseudo-first-order low apparently, with As(V) fitting better than As(III) in terms of the values of R^2.

The experimental data shown in Figure S6.a strongly align with the Elovich model, commonly employed to characterize chemisorption phenomena. Additionally, the regression coefficients (R^2) for As(III) and As(V) are notably higher compared to other kinetic models, with values of 0.9971 and 0.9672, respectively. This indicates that the adsorption of As(III) and As(V) onto Fe-SBE/C can be more appropriately described by a chemical adsorption mechanism involving chemical reactions. The significant R^2 values obtained from the Elovich model imply that the adsorption of As onto Fe-SBE/C is a complex process that entails the formation of chemical bonds. The adsorption rate is initially high but gradually decreases as the available adsorption sites diminish. This favorable model fit suggests that the adsorption process involves interactions at the atomic or molecular level, such as surface complexation or ion exchange, which indicate a chemisorption mechanism.

Table 3. The parameters of arsenic adsorption kinetic study.

Type of Kinetic	Parameter	As(III)	As(V)
Pseudo-first-order	qe_{exp} (μg g^{-1})	36.8077	27.9422
	qe_{cal} (μg g^{-1})	33.898	25.215
	k_1	0.1064	0.0536
	R^2	0.8396	0.9354
Elovich model	α (μg g^{-1} min)	0.1852	0.2039
	β (μg g^{-1})	1.7652	0.3402
	R^2	0.9971	0.9672
Intraparticle diffusion model 1	K_{diff} (μg $g^{-1/2})^{-1}$	4.6063	3.4548
	C (μg g^{-1})	5.5599	0.2689
	R2	0.9568	0.9797
Intraparticle diffusion model 2	Kdiff (μg $g^{-1/2})^{-1}$	0.8527	1.3477
	C (μg g^{-1})	25.8081	10.3075
	R^2	0.9318	0.9671

Based on the presented kinetic model in Figure S6d, the graph depicting qt versus $t^{1/2}$ for Fe-SBE/C demonstrates a multi-linear pattern with two distinct phases. Notably, the initial phase of the curves does not intersect with the origin, suggesting that intraparticle diffusion is not the only mechanism controlling the process. This implies that other factors, such as external mass transfer or chemisorption, are also involved. The intraparticle diffusion model analysis for Fe-SBE/C adsorbent reveals two distinct phases with their respective R^2 values. This indicates that although intraparticle diffusion contributed to the sorption process, it is not the exclusive mechanism involved. The present of a non-zero intercept (parameter C) in the model implies some level of boundary layer control. This suggests that the initial phase of adsorption may be influenced by the diffusion of As ions from the solution to the external surface of the adsorbent or film diffusion before intraparticle diffusion

 doi:10.20944/preprints202402.0685.v1

becomes significant. Overall, this model used in this work indicates that the As adsorption onto Fe-SBE/C is a complex process involving several steps or mechanisms.

2.2.6. Adsorption Isotherm

Figure S7 presents the plot of those three adsorption isotherm models for the adsorption As(III) and As(V). The corresponding values for the adsorption parameters can be found in Table 4. The suitability of the isotherm equation and the coefficient of determination (R^2) were compared. Notably, the Langmuir isotherm exhibited higher coefficients of determination (0.988 for As(III) and 0.9901 for As(V)) when compared to the Freundlich and Temkin isotherm. This suggests that the data obtained from the adsorption isotherm aligns more closely with the Langmuir model. Moreover, it implies that the composite surface had limited active sites, forming a monolayer of As(III) and As(V) over a homogeneous composite surface. The maximum adsorption capacity of Fe-SBE/C for As(III) and As(V) was determined to be 202.61 and 187.61 μg g^{-1}, respectively.

The Freundlich model yielded 1/n value ranging from 0 to 1, indicating favorable adsorption with strong interaction between the adsorbate and adsorbent. The maximum values of n for the adsorption process were determined to be 1.54 and 1.42, suggesting that adsorption becomes a non-physical phenomenon when n>1. These findings align with the Temkin isotherm model, suggesting that the interaction between the sorbate (As(III) and As(V) and the sorbent (Fe-SBE/C) leads to the surface complex formation involving the As(III)/As(V) anions. On the Fe-SBE/C surface, these complexes can occur as either monodentate or bidentate species. A ligand exchange occurs in both forms where As anions replace hydroxyl or other groups bound to iron oxide. The distinction between monodentate and bidentate complexes lies in their formation kinetics and the resulting structure of bonded surface species.

Table 4. Adsorption isotherm parameters.

Type of Isotherm	Parameters	As(III)	As(V)
Langmuir	Q_{max} (μg g^{-1})	202.61	187.61
	K_L (L μg^{-1})	0.0173	0.0078
	R^2	0.988	0.9901
Freundlich	K_F	7.2754	3.1061
	1/n	0.6486	0.7069
	R^2	0.978	0.9722
Temkin	B (J mol^{-1})	26.8809	32.0069
	A (L g^{-1})	0.5094	0.1203
	R^2	0.8830	0.9683

2.2.7. Adsorption Thermodynamics

The results depicted in Figure S8 demonstrate that the acquired values from the linear plot between $\ln K_L$ and 1/T, namely the slope and intercept, can be utilized to ascertain the alterations in entropy and enthalpy associated with As adsorption. The corresponding values at three different temperatures can be found in Table 5. The feasibility of the adsorption of As species on the adsorbent is confirmed as evidenced by the negative value of ΔG^o. On the other hand, as mentioned by Maiti et al. [48], the positive values of ΔS^o indicate the spontaneity of the adsorption process. Furthermore, the positive value of ΔH^o suggests that both arsenic species adsorption is endothermic in nature [49].

Additionally, apparent activation energy (E_a) of As(III)/As(V) adsorption were determined with the method as outlined in Text S1.4. Results of the Arrhenius plots are presented in Figure S9, and the determined Ea values are listed in Table 5, which demonstrate that As(III) possesses a significantly higher Ea (65.799 kJ mol^{-1}) compared to As(V) (21.009 kJ mol^{-1}). This observation

 doi:10.20944/preprints202402.0685.v1

indicates that the Ea for As adsorption exceeds the values reported by A. Ramesh et al. [50] and Mahmood et al. [51]. While Cantu et al. [52] have posited that adsorption reactions are categorized as chemisorption if the Ea exceeds 40 kJ mol^{-1}, whereas reactions with Ea below this demarcation are identified as physisorption. Based on the aforementioned Ea values for As(III) and As(V), it is inferred that the adsorption reaction involving As(III) is chemisorption, necessitating a significantly higher amount of energy compared to the adsorption of As(V). The lower Ea value associated with As(V) suggests that its reaction encounters fewer energy barriers, facilitating a more straightforward adsorption of As(V) onto Fe-SBE/C [53]. Nonetheless, Unuabonah et al. [54] have highlighted that physisorption typically occur with Ea values below 4.2 kJ mol^{-1}. This assertion is based on kinetic data, which ultimately suggests that the reactions occurring during the adsorption of As(III) and As(V) are indeed chemisorption reactions. Importantly, the adsorption process of As(V) occurs at a solution pH of 3, below its point of zero charge (pH_{PZC}), which enhances its interaction with the surface charges of the Fe-SBE/C, underscoring the influence of physicochemical properties on the adsorption dynamics.

Table 5. Thermodynamic parameter.

Thermodynamic Parameter	Temperature	As(III)	As(V)
ΔG^o (kJ mol^{-1})	25 °C	-2.298	-8.472
	35 °C	-2.576	-8.825
	40 °C	-2.677	-9.015
ΔH^o (kJ mol^{-1})		5.351	2.266
ΔS^o (J $mol^{-1}K^{-1}$)		25.682	36.0276
Ea (kJ mol^{-1})		65.799	21.009

2.3. Regeneration and Reusability Study

The reusability of Fe-SBE/C as a potential adsorbent was investigated through the adsorption-desorption method, explicitly focusing on the regeneration of Fe-SBE/C loaded arsenic. The regeneration process was conducted by utilizing 0.1 M NaOH as the regeneration agent, as it possesses the ability to induce electrostatic repulsion between the negatively charged adsorbent and the anionic form of arsenic [55]. The regeneration process resulted in three consecutive cycles, as illustrated in Figure S10. The graph depicts a decline in the regeneration and cycle studies. After the first cycle, the As(III) removal percentage gradually decreased from 74.91% to 65.87%. Further, it declined to 61.34% and 50.79% in the second and third cycles, respectively, under neutral pH conditions.

In contrast, the removal percentage of As(V) exhibited a notably superior outcome compared to As(III) when performed under its optimal pH condition of 3. However, the removal percentage gradually decreased from 93.63% to 87.17% after the first cycle and continued to decline to 77.91% after the third cycle. This discrepancy can be attributed to the slow removal rate of As(V) adsorption under neutral pH (7) conditions. The diminished efficacy of arsenic removal during the regeneration cycle can be ascribed to the insufficient regeneration procedure, leading to a decrease in the availability of sorption sites. These results indicate the necessity for additional investigation to enhance the regeneration process.

3. Materials and Methods

3.1. Chemicals

The SBE was provided by PT. Energy Unggul Persada-KPN Corp. (Indonesia). The chemicals used for the research, including Sodium arsenite ($NaAsO_2$) with a purity of 99.5%, were obtained

 doi:10.20944/preprints202402.0685.v1

from Xiya Reagent Center, Chengdu, China. Sodium arsenate ($Na_2HAsO_4.7H_2O$) with 98% purity was procured from Alfa Aesar Chemical Co., Ltd., Tianjin, China. Additionally, Ferric chloride ($FeCl_3•6H_2O$), ferrous chloride ($FeCl_2.H_2O$), and 25% ammonia solution (NH_3OH), Sodium hydroxide (NaOH), Hydrochloric acid (HCl), and Potassium hydroxide (KOH), along with other necessary chemicals, were obtained from Sinopharm Chemical Reagent Co., Ltd., Shanghai, China. Potassium borohydride (KBH_4) was obtained from Shanghai Lingfeng Chemicals Reagent Co.Ltd. The chemicals used in this work are of reagent grade or analytical grade. For all procedures of experiment, ultra-pure water with 18 Ω cm^{-1} of resistivity was produced by a water purification system from Sichuan Youpu Ultrapure Technology Co. ltd., Sichuan, China. The solutions prepared for this study were stored at 4 °C.

3.2. Preparation of the Materials

3.2.1. Preparation of SBE/C Composite

The SBE/C was synthesized via calcination using a muffle furnace, following the methodology outlined by Tang et al. [21]. Initially, a weighted sample of SBE of around 25 grams was subjected to calcination at temperatures of 350, 400, 450, 500, and 550 °C. The calcination process was carried out in an air atmosphere, reaching the desired final temperature and maintaining it for two hours. The calcination process was ranged from 1 to 3 hours to observe the efficiency of holding time calcination. The resulting samples were systematically named SBE/Cx,y, with 'x' denoting the specific calcination temperature and 'y' indicating the holding time, respectively.

3.2.2. Modification of Iron-Loaded Spent Bleaching Earth (Fe-SBE/C)

The Fe-SBE/C, a magnetic material, was synthesized using the co-precipitation technique described by Jiali et al. [56]. The process began with preparing a 100 mL iron solution containing $FeCl_3.6H_2O$ and $FeCl_2.4H_2O$ with a ratio of 2:1.5 (w/w). This solution was heated in a 500 mL beaker under constant stirring until it reached 90 °C, at which point the solution's color transitioned from transparent orange to milky orange. The pH of this solution was then carefully adjusted to between 9 and 10 using a 35% ammonia solution and added dropwise to precipitate the iron ions. After complete dissolution, 2.0 grams of prepared SBE/C were introduced and stirred for 60 minutes at a temperature of 90 °C using a magnetic stirrer with consistent heating. The dark black solution is cooled to room temperature and filtered using ultra-pure water under vacuum filtration. It is subsequently washed three times. Later, the solid was dehydrated in an oven at 378 K for one hour. The final product, Fe-SBE/Cx,y, is named according to the temperature (x) and duration (y) of the calcination process used for the initial SBE/C. Different molar ratios of Fe^{+3} to Fe^{+2} (1:1, 1:1.5, and 1:2) were utilized to achieve the desired iron loading on the magnetic-SBE/C composite.

3.2.3. Adsorption of As(III) and As(V) Studies

Generally, the adsorption experiments were conducted by placing glass bottles with sealed lids in a water bath rotary shaker. The temperature was maintained at a constant level of 25±2 ℃. About 250 mL of 50 μg L^{-1} of As(III) or As(V) was supplemented with 1 g/L of Fe-SBE/C composite in a glass bottle with the lid on. The solution's pH was modified until reaching the intended level using 0.1 M HCl or NaOH solution. The experiment was conducted in duplicate, and the sample underwent agitation in a water bath rotary shaker at 250 rpm. The mixture was collected about 4.5 mL at regular intervals throughout the reaction. A sample was obtained by passing the mixture through a 0.22 μm polyethersulfone (PES) filter and pouring it into a plastic tube. Ultimately, As(III) or As(V) in the solution was determined by using a hydride-generation atomic fluorescence spectrophotometer (HG-AFS).

The efficiency of adsorption removal was determined by the equation below:

$$\text{Removal efficiency} = \frac{C_0 - C_e}{C_0} \times 100\% \quad (1)$$

 doi:10.20944/preprints202402.0685.v1

where C_0 represents the initial and C_e, the final concentrations of arsenic in the solution, respectively. Subsequently, the subsequent equation was employed to ascertain the adsorption capacity q_e (μg g^{-1}):

$$q_e = \frac{(C_0 - C_e) \times V}{M} \quad (2)$$

where C_0 and Ce are the same as that in Equation (1), V represents the volume of the solution (L), while M is the quantity of used adsorbent for adsorption (gram) [21].

A series of experiments were conducted to investigate the impact of different chemical factors on the adsorption efficiency of As(III) and As(V). These experiments involved varying the ratio of iron(III) and iron(II) at molar ratios 0.5:0.5, 1:1, 1.5:1.5, and 2:2; adjusting the pH of solution within the range of 3-10, utilization of adsorbent doses ranging from 0.5- 250 μg L^{-1}; the introducing of co-existing ion including chloride, sulfate, carbonate, and phosphate.

Other experiment methods including characterization with Fourier transform infrared spectra (FTIR), X-ray diffraction pattern (XRD), Field emission scanning electron microscope and energy dispersive X-ray spectroscopy (SEM-EDS), BET surface area and distribution of pore size, thermogravimetric analysis (TGA), points of zero charge (PZC) analysis, magnetic hysteresis curve, detection of As(III) and As(V) with HG-AFS, kinetic analysis and thermodynamics (isotherm curves, and Arrhenius equation) of the adsorption are provided in the Supplementary Materials (Text S1).

4. Conclusions

In summary, this study presents a comprehensive investigation on the adsorption of As(III) and As(V) by Fe-SBE/C composite produced by the co-precipitation method. Fe-SBE/C material is suitable as an adsorbent for both As(III) and As(V) removal, with promising characteristics such as an expanded specific surface area from 191.19 to 2865.7 m^2 g^{-1}. The adsorption process is primarily chemisorption, where the reaction factor plays a significant role in the interaction between As and Fe-SBE/C, including surface complexation and electrostatic attraction (mainly for As(V)) occurring on the Fe-SBE/C surface. Overall, this work successfully demonstrates the modification of SBE, resulting in improved physicochemical properties that enhance its efficacy as an adsorbent for inorganic As. The findings highlight the potential of environmentally-friendly adsorbents as cost-effective, efficient, and recyclable products produced through sustainable processes.

Supplementary Materials: The following supporting information can be downloaded at: www.mdpi.com/xxx/ Text S1: Physicochemical characterization of material and methods; Figure S1: FTIR spectra for (a) and (b) the raw and modified materials; Figure S2: The energy-dispersive X-ray spectroscopy (EDS) element in the material; Figure S3: (a) Adsorption and desorption curves of N_2, (b) distribution of pore size; Figure S4: Comparison of arsenic removal between SBE/C 500 °C-3h, Fe_3O_4, and Fe-SBE/C 500 °C; Figure S5: The influences of a.c) adsorbent dosage, b.d) ratio of Fe^{+3}/Fe^{+2} on arsenic adsorption; Figure S6: Adsorption kinetic studies of As(III) and As(V); Figure S7:Isotherm Langmuir, Freundlich, and Temkin model of As(III) and As(V) adsorption; Figure S8: Adsorption thermodynamic (Van't Hoff) plot; Figure S9: Arrhenius plot of As(III) and As(V) adsorption; Figure S10: Reusability cycle of Fe-SBE/C for As(III) and As(V) adsorption.

Author Contributions: Siswanti Puji: investigation, writing original draft, visualization; Juntao Guo: investigation, writing-review and editing, and formal analysis; Yihui Zhang: investigation, formal analysis; Kexin Song: investigation, formal analysis; Feng Wu: Supervision, writing-review and editing, project administration; Jing Li: Resources, review and editing.

Funding: China Scholarship Council (CSC) No: 2019GBJ002047.

Data Availability Statement: Data is contained within the article.

Acknowledgments: This work was financially supported by the School of International Education and School of Resources and Environmental Science, Wuhan University. The authors thank PT. Energy Unggul Persada-KPN Corp. from Indonesia for providing the raw material of SBE.

Conflicts of Interest: The authors declare no conflict of interest.

Sample Availability: The SBE used in the study was provided by PT. Energy Unggul Persada-KPN Corp. (Indonesia).

References

1. USEPA 2002 Edition of the Drinking Water Standards and Health Advisories 2002 Edition of the Drinking Water Standards and Health Advisories. **2002**, 19.
2. Fendorf, S.; Kocar, B.D. Chapter 3 Biogeochemical Processes Controlling the Fate and Transport of Arsenic. Implications for South and Southeast Asia. *Adv. Agron.* **2009**, *104*, 137–164. https://doi.org/10.1016/S0065-2113(09)04003-6.
3. Ghorbanzadeh, N.; Jung, W.; Halajnia, A.; Lakzian, A.; Kabra, A.N.; Jeon, B.H. Removal of Arsenate and Arsenite from Aqueous Solution by Adsorption on Clay Minerals. *Geosystem Eng.* **2015**, *18*, 302–311. https://doi.org/10.1080/12269328.2015.1062436.
4. Bhowmick, S.; Pramanik, S.; Singh, P.; Mondal, P.; Chatterjee, D.; Nriagu, J. Arsenic in Groundwater of West Bengal, India: A Review of Human Health Risks and Assessment of Possible Intervention Options. *Sci. Total Environ.* **2018**, *612*, 148–169. https://doi.org/10.1016/j.scitotenv.2017.08.216.
5. Podgorski, J.; Berg, M. Global Threat of Arsenic in Groundwater. *Science (80-.).* **2020**, *368*, 845–850. https://doi.org/10.1126/science.aba1510.
6. World Health Organization Guidelines for Drinking Water Quality. International Standard for Drinking Water Guidelines for Water Quality. **2011**, 1–2.
7. Páez-Espino, D.; Tamames, J.; de Lorenzo, V.; Cánovas, D. Microbial Responses to Environmental Arsenic. *BioMetals* **2009**, *22*, 117–130. https://doi.org/10.1007/s10534-008-9195-y.
8. Ungureanu, G.; Santos, S.; Boaventura, R.; Botelho, C. Arsenic and Antimony in Water and Wastewater: Overview of Removal Techniques with Special Reference to Latest Advances in Adsorption. *J. Environ. Manage.* **2015**, *151*, 326–342. https://doi.org/10.1016/j.jenvman.2014.12.051.
9. Luo, T.; Xu, J.; Li, J.; Wu, F.; Zhou, D. Strengthening Arsenite Oxidation in Water Using Metal-Free Ultrasonic Activation of Sulfite. *Chemosphere* **2021**, *281*. https://doi.org/10.1016/j.chemosphere.2021.130860.
10. Kobya, M.; Soltani, R.D.C.; Omwene, P.I.; Khataee, A. A Review on Decontamination of Arsenic-Contained Water by Electrocoagulation: Reactor Configurations and Operating Cost along with Removal Mechanisms. *Environ. Technol. Innov.* **2020**, *17*. https://doi.org/10.1016/j.eti.2019.100519.
11. Rathi, B.S.; Kumar, P.S.; Ponprasath, R.; Rohan, K.; Jahnavi, N. An Effective Separation of Toxic Arsenic from Aquatic Environment Using Electrochemical Ion Exchange Process. *J. Hazard. Mater.* **2021**, *412*. https://doi.org/10.1016/j.jhazmat.2021.125240.
12. Baigorria, E.; Cano, L.; Sapag, K.; Alvarez, V. Removal Efficiency of As(III) from Aqueous Solutions Using Natural and Fe(III) Modified Bentonites. *Environ. Technol. (United Kingdom)* **2022**, *43*, 3728–3741. https://doi.org/10.1080/09593330.2021.1934559.
13. Silerio-Vázquez, F.; Proal Nájera, J.B.; Bundschuh, J.; Alarcon-Herrera, M.T. Photocatalysis for Arsenic Removal from Water: Considerations for Solar Photocatalytic Reactors. *Environ. Sci. Pollut. Res.* **2022**, *29*, 61594–61607. https://doi.org/10.1007/s11356-021-16507-5.
14. Baigorria, E.; Cano, L.; Alvarez, V.A. Nanoclays as Eco-Friendly Adsorbents of Arsenic for Water Purification. *Handb. Nanomater. Nanocomposites Energy Environ. Appl. Vol. 1-4* **2021**, *1*, 455–470. https://doi.org/10.1007/978-3-030-36268-3_61.
15. Caroni, A.L.P.F.; de Lima, C.R.M.; Pereira, M.R.; Fonseca, J.L.C. Tetracycline Adsorption on Chitosan: A Mechanistic Description Based on Mass Uptake and Zeta Potential Measurements. *Colloids Surfaces B Biointerfaces* **2012**, *100*, 222–228. https://doi.org/10.1016/j.colsurfb.2012.05.024.
16. Liu, Y.; Li, J.; Wu, L.; Shi, Y.; He, Q.; Chen, J.; Wan, D. Magnetic Spent Bleaching Earth Carbon (Mag-SBE@C) for Efficient Adsorption of Tetracycline Hydrochloride: Response Surface Methodology for Optimization and Mechanism of Action. *Sci. Total Environ.* **2020**, *722*. https://doi.org/10.1016/j.scitotenv.2020.137817.
17. Mukhopadhyay, R.; Manjaiah, K.M.; Datta, S.C.; Yadav, R.K.; Sarkar, B. Inorganically Modified Clay Minerals: Preparation, Characterization, and Arsenic Adsorption in Contaminated Water and Soil. *Appl. Clay Sci.* **2017**, *147*, 1–10. https://doi.org/10.1016/j.clay.2017.07.017.
18. Loh, S.K.; Cheong, K.Y.; Salimon, J. Surface-Active Physicochemical Characteristics of Spent Bleaching Earth on Soil-Plant Interaction and Water-Nutrient Uptake: A Review. *Appl. Clay Sci.* **2017**, *140*, 59–65. https://doi.org/10.1016/j.clay.2017.01.024.
19. Tsai, W.T.; Chang, Y.M.; Lai, C.W.; Lo, C.C. Adsorption of Ethyl Violet Dye in Aqueous Solution by Regenerated Spent Bleaching Earth. *J. Colloid Interface Sci.* **2005**, *289*, 333–338. https://doi.org/10.1016/j.jcis.2005.03.087.
20. Eko Saputro, K.; Siswanti, P.; Wahyu Nugroho, D.; Ikono, R.; Noviyanto, A.; Taufiqu Rochman, N. Reactivating Adsorption Capacities of Spent Bleaching Earth for Using in Crude Palm Oil Industry. *IOP Conf. Ser. Mater. Sci. Eng.* **2020**, *924*. https://doi.org/10.1088/1757-899X/924/1/012014.
21. Tang, J.; Mu, B.; Zheng, M.; Wang, A. One-Step Calcination of the Spent Bleaching Earth for the Efficient Removal of Heavy Metal Ions. *ACS Sustain. Chem. Eng.* **2015**, *3*, 1125–1135. https://doi.org/10.1021/acssuschemeng.5b00040.

22. Liu, W.; Yuan, K.; Yin, K.; Zuo, S.; Yao, C. Clay-Activated Carbon Adsorbent Obtained by Activation of Spent Bleaching Earth and Its Application for Removing Pb(II) Ion. *Environ. Sci. Pollut. Res.* **2021**, *28*, 711–723. https://doi.org/10.1007/s11356-020-10473-0.
23. Wan, D.; Wan, H.; Shi, Y.; Jin, J.; Zhang, Z.; Lu, J. Enhanced Removal of Sb(V) by Iron-spent Bleaching Earth Carbon Binary Micro-electrolysis System: Performance and Mechanism. *J. Chem. Technol. Biotechnol.* **2023**, *98*, 2181–2191. https://doi.org/10.1002/jctb.7431.
24. Wan, D.; Chen, Y.; Shi, Y.; Liu, Y.; Xiao, S. Effective Adsorption of Bisphenol A from Aqueous Solution over a Novel Mesoporous Carbonized Material Based on Spent Bleaching Earth. *Environ. Sci. Pollut. Res.* **2021**, *28*, 40035–40048. https://doi.org/10.1007/s11356-021-13596-0.
25. Liu, L.; Li, Y.; Yoza, B.A.; Hao, K.; Li, Q.X.; Li, Y.; Wang, Q.; Guo, S.; Chen, C. A Char-Clay Composite Catalyst Derived from Spent Bleaching Earth for Efficient Ozonation of Recalcitrants in Water. *Sci. Total Environ.* **2020**, *699*. https://doi.org/10.1016/j.scitotenv.2019.134395.
26. Chen, Y.; Shi, Y.; Wan, D.; Zhao, J.; He, Q.; Liu, Y. Synergistic Adsorption and Advanced Oxidation Activated by Persulfate for Degradation of Tetracycline Hydrochloride Using Iron-Modified Spent Bleaching Earth Carbon. *Environ. Sci. Pollut. Res.* **2022**, *29*, 24704–24715. https://doi.org/10.1007/s11356-021-17435-0.
27. Almasri, D.A.; Rhadfi, T.; Atieh, M.A.; McKay, G.; Ahzi, S. High Performance Hydroxyiron Modified Montmorillonite Nanoclay Adsorbent for Arsenite Removal. *Chem. Eng. J.* **2018**, *335*, 1–12. https://doi.org/10.1016/j.cej.2017.10.031.
28. Sanaei, L.; Tahmasebpoor, M.; Khatamian, M.; Divband, B. Arsenic Removal from Aqueous Solutions Using Iron Oxide-Modified Zeolite: Experimental and Modeling Investigations. *AUT J. Mech. Eng.* **2021**, *5*, 141–152. https://doi.org/10.22060/ajme.2020.17214.5849.
29. Linh, N.L.M.; Hoang Van, D.; Duong, T.; Tinh, M.X.; Khieu, D.Q. Adsorption of Arsenate from Aqueous Solution onto Modified Vietnamese Bentonite. *Adv. Mater. Sci. Eng.* **2019**, *2019*. https://doi.org/10.1155/2019/2710926.
30. Tuutijärvi, T.; Lu, J.; Sillanpää, M.; Chen, G. As(V) Adsorption on Maghemite Nanoparticles. *J. Hazard. Mater.* **2009**, *166*, 1415–1420. https://doi.org/10.1016/j.jhazmat.2008.12.069.
31. Asere, T.G.; Stevens, C. V.; Du Laing, G. Use of (Modified) Natural Adsorbents for Arsenic Remediation: A Review. *Sci. Total Environ.* **2019**, *676*, 706–720. https://doi.org/10.1016/j.scitotenv.2019.04.237.
32. Aftabtalab, A.; Rinklebe, J.; Shaheen, S.M.; Niazi, N.K.; Moreno-Jiménez, E.; Schaller, J.; Knorr, K.-H. Review on the Interactions of Arsenic, Iron (Oxy)(Hydr)Oxides, and Dissolved Organic Matter in Soils, Sediments, and Groundwater in a Ternary System. *Chemosphere* **2022**, *286*, 131790. https://doi.org/10.1016/j.chemosphere.2021.131790.
33. Tang, J.; Zong, L.; Mu, B.; Kang, Y.; Wang, A. Attapulgite/Carbon Composites as a Recyclable Adsorbent for Antibiotics Removal. *Korean J. Chem. Eng.* **2018**, *35*, 1650–1661. https://doi.org/10.1007/s11814-018-0066-0.
34. Barakat, M.A.; Kumar, R.; Halawani, R.F.; Al-Mur, B.A.; Seliem, M.K. Fe_3O_4 Nanoparticles Loaded Bentonite/Sawdust Interface for the Removal of Methylene Blue: Insights into Adsorption Performance and Mechanism via Experiments and Theoretical Calculations. *Water* **2022**, *14*, 3491. https://doi.org/10.3390/w14213491.
35. Chen, L.; Huang, Y.; Huang, L.; Liu, B.; Wang, G.; Yu, S. Characterization of Co(II) Removal from Aqueous Solution Using Bentonite/Iron Oxide Magnetic Composites. *J. Radioanal. Nucl. Chem.* **2011**, *290*, 675–684. https://doi.org/10.1007/s10967-011-1337-y.
36. Mu, B.; Wang, A. One-Pot Fabrication of Multifunctional Superparamagnetic Attapulgite/Fe_3O_4/Polyaniline Nanocomposites Served as an Adsorbent and Catalyst Support. *J. Mater. Chem. A* **2015**, *3*, 281–289. https://doi.org/10.1039/c4ta05367b.
37. Morin, G.; Wang, Y.; Ona-Nguema, G.; Juillot, F.; Calas, G.; Menguy, N.; Aubry, E.; Bargar, J.R.; Brown, G.E. EXAFS and HRTEM Evidence for As(III)-Containing Surface Precipitates on Nanocrystalline Magnetite: Implications for as Sequestration. *Langmuir* **2009**, *25*, 9119–9128. https://doi.org/10.1021/la900655v.
38. Su, H.; Ye, Z.; Hmidi, N. High-Performance Iron Oxide–Graphene Oxide Nanocomposite Adsorbents for Arsenic Removal. *Colloids Surfaces A Physicochem. Eng. Asp.* **2017**, *522*, 161–172. https://doi.org/10.1016/j.colsurfa.2017.02.065.
39. Kumar, A.S.K.; Jiang, S.J. Synthesis of Magnetically Separable and Recyclable Magnetic Nanoparticles Decorated with β-Cyclodextrin Functionalized Graphene Oxide an Excellent Adsorption of As(V)/(III). *J. Mol. Liq.* **2017**, *237*, 387–401. https://doi.org/10.1016/j.molliq.2017.04.093.
40. Das, T.K.; Bezbaruah, A.N. Comparative Study of Arsenic Removal by Iron-Based Nanomaterials: Potential Candidates for Field Applications. *Sci. Total Environ.* **2021**, *764*. https://doi.org/10.1016/j.scitotenv.2020.142914.

41. Repo, E.; Mäkinen, M.; Rengaraj, S.; Natarajan, G.; Bhatnagar, A.; Sillanpää, M. Lepidocrocite and Its Heat-Treated Forms as Effective Arsenic Adsorbents in Aqueous Medium. *Chem. Eng. J.* **2012**, *180*, 159–169. https://doi.org/10.1016/j.cej.2011.11.030.
42. Joshi, S.; Sharma, M.; Kumari, A.; Shrestha, S.; Shrestha, B. Arsenic Removal from Water by Adsorption onto Iron Oxide/Nano-Porous Carbon Magnetic Composite. *Appl. Sci.* **2019**, *9*, 3732. https://doi.org/10.3390/app9183732.
43. Mudzielwana, R.; Gitari, M.W.; Ndungu, P. Performance Evaluation of Surfactant Modified Kaolin Clay in As(III) and As(V) Adsorption from Groundwater: Adsorption Kinetics, Isotherms and Thermodynamics. *Heliyon* **2019**, *5*. https://doi.org/10.1016/j.heliyon.2019.e02756.
44. Penke, Y.K.; Yadav, A.K.; Malik, I.; Tyagi, A.; Ramkumar, J.; Kar, K.K. Insights of Arsenic (III/V) Adsorption and Electrosorption Mechanism onto Multi Synergistic (Redox-Photoelectrochemical-ROS) Aluminum Substituted Copper Ferrite Impregnated RGO. *Chemosphere* **2021**, *267*. https://doi.org/10.1016/j.chemosphere.2020.129246.
45. Zhang, G.; Liu, H.; Liu, R.; Qu, J. Adsorption Behavior and Mechanism of Arsenate at Fe–Mn Binary Oxide/Water Interface. *J. Hazard. Mater.* **2009**, *168*, 820–825. https://doi.org/10.1016/j.jhazmat.2009.02.137.
46. Bullen, J.C.; Saleesongsom, S.; Gallagher, K.; Weiss, D.J. A Revised Pseudo-Second-Order Kinetic Model for Adsorption, Sensitive to Changes in Adsorbate and Adsorbent Concentrations. *Langmuir* **2021**, *37*, 3189–3201. https://doi.org/10.1021/acs.langmuir.1c00142.
47. Xiao, Y.; Azaiez, J.; Hill, J.M. Erroneous Application of Pseudo-Second-Order Adsorption Kinetics Model: Ignored Assumptions and Spurious Correlations. *Ind. Eng. Chem. Res.* **2018**, *57*, 2705–2709. https://doi.org/10.1021/acs.iecr.7b04724.
48. Maiti, A.; DasGupta, S.; Basu, J.K.; De, S. Adsorption of Arsenite Using Natural Laterite as Adsorbent. *Sep. Purif. Technol.* **2007**, *55*, 350–359. https://doi.org/10.1016/j.seppur.2007.01.003.
49. Wu, Y.H.; Li, B.; Feng, S.X.; Mi, X.M.; Jiang, J.L. Adsorption of Cr(VI) and As(III) on Coaly Activated Carbon in Single and Binary Systems. *Desalination* **2009**, *249*, 1067–1073. https://doi.org/10.1016/j.desal.2009.06.049.
50. Ramesh, A.; Hasegawa, H.; Maki, T.; Ueda, K. Adsorption of Inorganic and Organic Arsenic from Aqueous Solutions by Polymeric Al / Fe Modified Montmorillonite. **2007**, *56*, 90–100. https://doi.org/10.1016/j.seppur.2007.01.025.
51. Mahmood, T.; Din, S.U.; Naeem, A.; Tasleem, S.; Alum, A.; Mustafa, S. Kinetics, Equilibrium and Thermodynamics Studies of Arsenate Adsorption from Aqueous Solutions onto Iron Hydroxide. *J. Ind. Eng. Chem.* **2014**, *20*, 3234–3242. https://doi.org/10.1016/j.jiec.2013.12.004.
52. Cantu, Y.; Remes, A.; Reyna, A.; Martinez, D.; Villarreal, J.; Ramos, H.; Trevino, S.; Tamez, C.; Martinez, A.; Eubanks, T.; et al. Thermodynamics, Kinetics, and Activation Energy Studies of the Sorption of Chromium(III) and Chromium(VI) to a Mn3O4 Nanomaterial. *Chem. Eng. J.* **2014**, *254*, 374–383. https://doi.org/10.1016/j.cej.2014.05.110.
53. Ebelegi, A.N.; Ayawei, N.; Wankasi, D. Interpretation of Adsorption Thermodynamics and Kinetics. *Open J. Phys. Chem.* **2020**, *10*, 166–182. https://doi.org/10.4236/ojpc.2020.103010.
54. Unuabonah, E.I.; Adebowale, K.O.; Olu-Owolabi, B.I. Kinetic and Thermodynamic Studies of the Adsorption of Lead (II) Ions onto Phosphate-Modified Kaolinite Clay. *J. Hazard. Mater.* **2007**, *144*, 386–395. https://doi.org/10.1016/j.jhazmat.2006.10.046.
55. Li, Z.; Deng, S.; Yu, G.; Huang, J.; Lim, V.C. As(V) and As(III) Removal from Water by a Ce–Ti Oxide Adsorbent: Behavior and Mechanism. *Chem. Eng. J.* **2010**, *161*, 106–113. https://doi.org/10.1016/j.cej.2010.04.039.
56. Chang, J.; Ma, J.; Ma, Q.; Zhang, D.; Qiao, N.; Hu, M.; Ma, H. Adsorption of Methylene Blue onto Fe_3O_4/Activated Montmorillonite Nanocomposite. *Appl. Clay Sci.* **2016**, *119*, 132–140. https://doi.org/10.1016/j.clay.2015.06.038.